This project has received funding from the European Union's Horizon 2020 research and innovation programme under grant agreement No 871813.

ICT Project No 871813

MUNDFAB

Modeling Unconventional Nanoscaled Device FABrication

D3.3: First batch of experimental results on epitaxy

R. Daubriac (CNRS), B. Sklenard (CEA), J.-M. Hartmann (CEA), P. Acosta Alba (CEA), S. Kerdiles (CEA), P. Michalowski (Łukasiewicz-IMiF), A. La Magna (CNR-IMM), F. Cristiano (CNRS)

August 26, 2021

Quality management

This deliverable was reviewed by:

Peter Pichler, Fraunhofer

Giuseppe Fisicaro, CNR-IMM

Contents

Abstract

Work package 3 covers the epitaxial growth of Si, SiGe and Ge heterostructures by chemical vapor deposition (CVD), which is widely used for the manufacturing of nanoelectronics materials (i.e. raised source/drain fabrication in FDSOI and FinFET technology) and which is also a keystone for future technologies based on these materials (i.e. gate-all-around transistors).

In order to improve the existing TCAD models for the predictive simulation of physical phenomena occurring during epitaxial growth, dedicated experiments have been planned within this WP, based on CVD grown SiGe layers with different Ge contents, thicknesses, strains and doping concentrations. This deliverable describes the results of the characterization of these layers with respect to thickness, germanium content, and strain state. The boron-doped layers were also characterized with respect to the chemical and electrically active dopant concentration. Finally, an experimental plan for the further annealing of epitaxially grown layers to increase the electrically active dopant fraction is presented.

Introduction

In this document, we present a detailed characterization of the as-grown SiGe layers that were available at the beginning of the project (cf. “first batch of samples”, deliverable D3.2, section 2, Fig. 1). Results related to the undoped SiGe layers are first reported in Section 1, while boron-doped SiGe layers will be described in Section 2. For each wafer, the germanium composition, layer thickness and strain level have been measured using different experimental methods.

The investigation of boron-doped wafers shows that the electrical activation rate of boron decreases when increasing the chemical concentration of dopants. A dedicated experiment designed to investigate the improvement of the dopant activation rate thanks to “low-thermal budget” annealing techniques (cf. Task 3.4) has therefore been planned. It will be described in the last section of this deliverable (Section 3). This experiment will be carried out on the new set of SiGe layers recently fabricated at CEA-Leti (cf. “second batch of samples”, deliverable D3.2, section 3, Fig. 2) which were made available to the MUNDFAB consortium.

1 Undoped SiGe epi-layers

1.1 Fabrication process

In this section, we focus on a subset of three strained SiGe layers with a nominal thickness of 30 nm and a Ge concentration of 20, 30 and 40 at. %, respectively. These parameters were selected in order to reproduce as faithfully as possible the epitaxy conditions that are typically used for the fabrication of raised source/drain regions in FD-SOI or FinFET technologies **[1]**. The initial wafers were p-type (100) bulk silicon 300 mm wafers. A 1100 °C, 2 min, H_2 bake was performed in the CVD chamber to remove the native oxide prior to epitaxy. After such a surface preparation, SiGe layers were deposited in between 600 °C and 700 °C, 20 Torr, a constant $F(SiH_2Cl_2)/F(H_2)$ mass-flow ratio (MFR) and various $F(GeH_4)/F(H_2)$ MFRs to obtain the desired Ge concentrations. It is also important to specify that these process conditions were selected after a considerable amount of optimizations on control wafers with similar features (thickness, *in-situ* doping, germanium content).

1.2 Optical analysis (XRR, XRD, ES)

After layer fabrication, various characterizations were conducted at CEA-Leti to determine the Ge concentrations and layer thicknesses including x-ray reflectivity (XRR), x-ray diffractometry (XRD) and spectroscopic ellipsometry (SE).

X-ray reflectometry (XRR) measurements

XRR measurements, performed at the center of each wafer, are presented in **Fig. 1.1**. Curves show clear fringes even at high incidence angles θ, highlighting the flatness of the SiGe surface and the abruptness of the SiGe/Si interface. In addition, as expected, the intensity of the fringes increases with the germanium content.

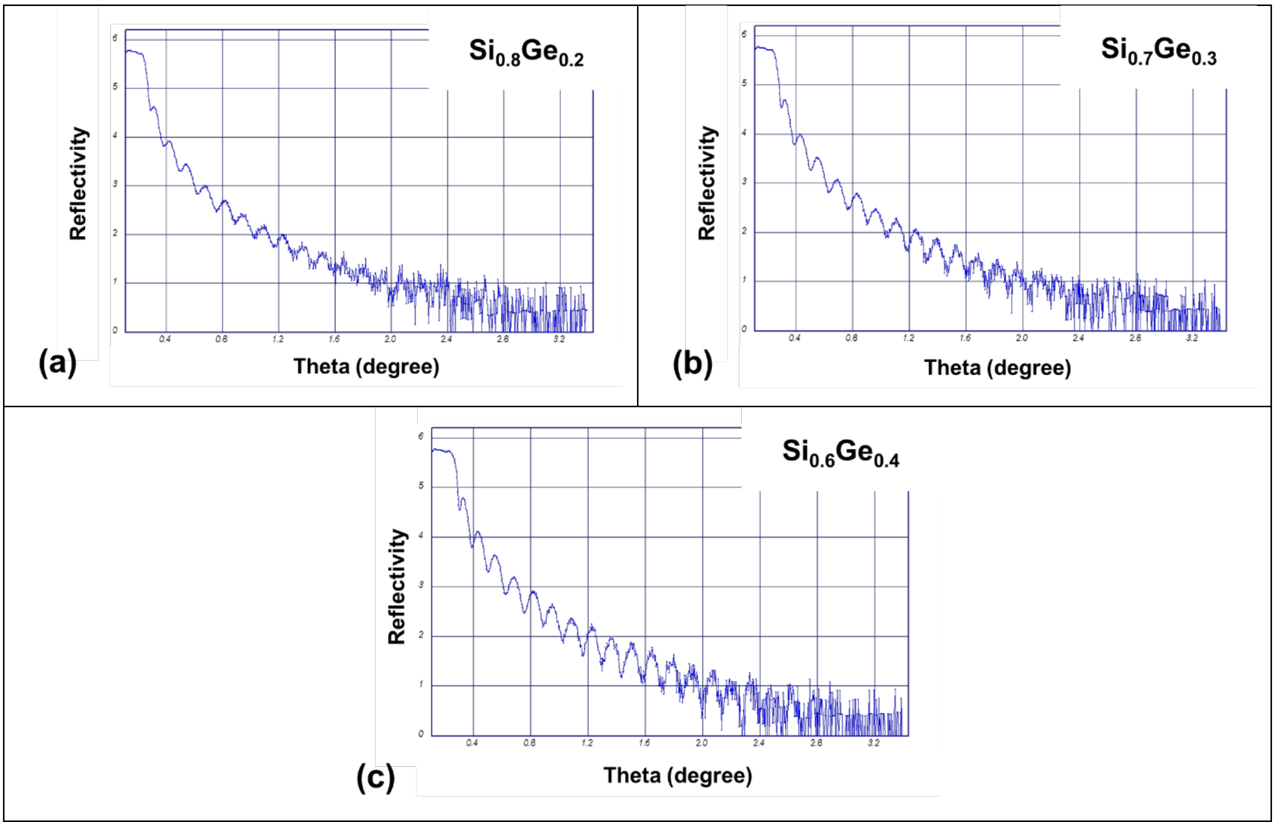

Figure 1.1: X-ray reflectivity curves for SiGe layers, with 20 % **(a)**, 30 % **(b)** and 40 % **(c)** of Ge (30 nm thick SiGe layers on Si(001) substrates).

Layer thicknesses can be calculated by applying fast Fourier transforms (FFT) on the collected profile. Those FFT give access to the native oxide/SiGe bilayer thickness. The uniformity of the wafers in terms of thickness was thus evaluated through FFTs on XRR profiles acquired on 9 points at 0 cm, 7 cm and 13 cm from the wafers' centres. Resulting thicknesses are summarized in **Tab. 1.1**. The uniformity is excellent, with average thicknesses of 30.7 nm, 30.3 nm and 30.9 nm for SiGe(20 %), SiGe(30 %) and SiGe(40 %) layers, respectively.

	Mean thickness (Å)			
Layers	**At 0 cm**	**At 7 cm**	**At 13 cm**	**Overall mean thickness (Å)**
SiGe (20 %)	310 ± 1.0 %	307.5 ± 0.2 %	305.7 ± 1.2 %	**307.0 ± 0.9 %**
SiGe (30 %)	306 ± 1.0 %	304.2 ± 0.5 %	300.7 ± 1.2 %	**302.9 ± 1.1 %**
SiGe (40 %)	312 ± 1.0 %	311.5 ± 0.2 %	306.0 ± 0.9 %	**309.1 ± 1.1 %**

Table 1.1: Thicknesses from FFT on XRR profiles (9 points polar maps at 0 cm, 7 cm and 13 cm from the wafer centers).

X-ray diffractometry analysis

In order to confirm that the Ge concentrations inside the different SiGe layers were close to the targeted ones, omega-2theta scans around the (004) x-ray diffraction (XRD) order were performed. **Fig. 1.2** profiles show well-defined and intense bulk Si peaks at 0 arcsec and SiGe layer peaks, with thickness fringes on both sides, which "move away" from the Si substrate peaks as the Ge content increases. Assuming that all layers were monocrystalline, simulations based on dynamical diffraction theory were carried out and thicknesses of 30.8 nm, 30.4 nm and 31.0 nm with Ge concentrations of 20.6 %, 30.4 % and 40.6 % were found for SiGe(20 %), SiGe(30 %) and SiGe(40 %) layers, respectively (errors on the thickness and on the germanium content are inferior to 1 nm and 1 %). These results are in very good agreement with the targeted values.

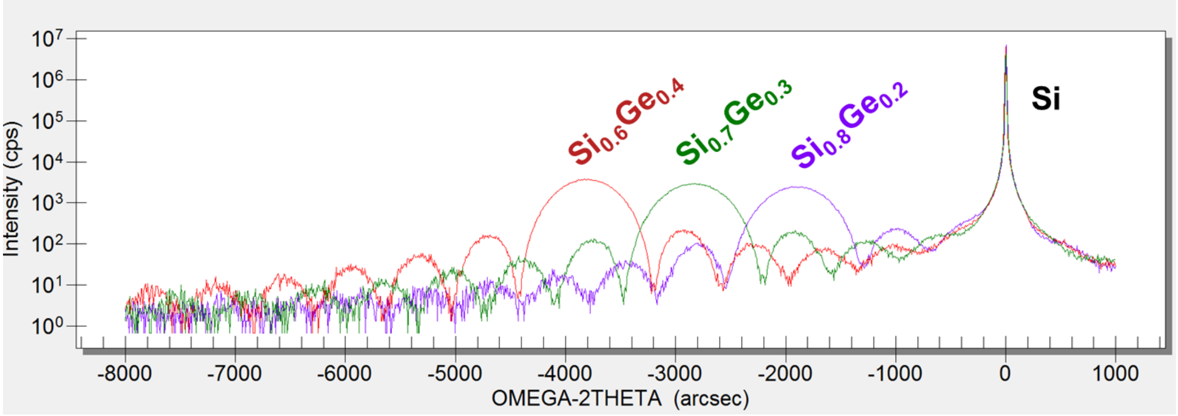

Figure 1.2: Omega-2Theta scans around the (004) XRD order for 30 nm thick SiGe layers, with 20 %, 30 % and 40 % on Si(001) substrates.

Spectroscopic Ellipsometry measurements

A final evaluation of the layer thickness and the Ge concentration uniformity was achieved thanks to spectroscopic ellipsometry, SE, although SE is a less precise characterization method compared to XRR and XRD. 49 points polar maps with 6 mm edge exclusions were acquired on the 3 wafers. Simulations gave us the layer thicknesses (**Fig. 1.3 (a-c)**) and Ge concentrations (**Fig. 1.3 (d-f)**).

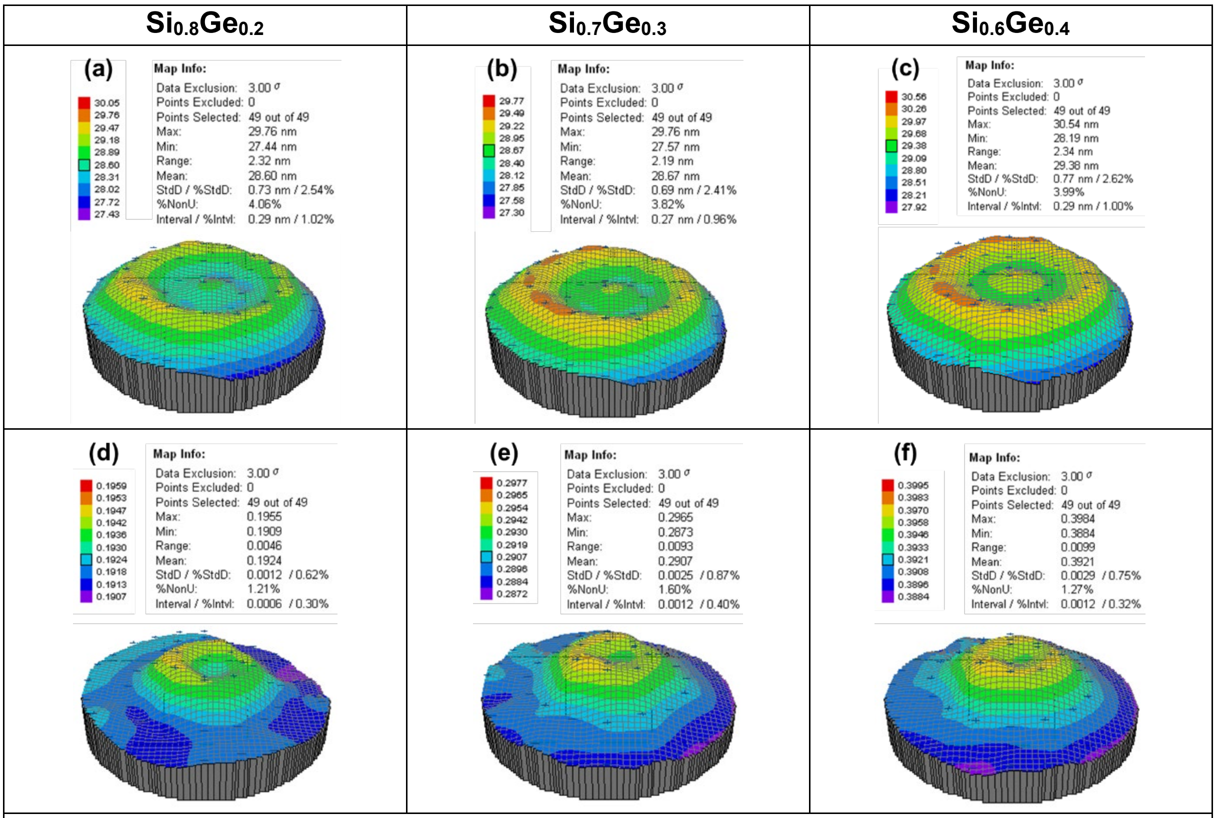

(a)
Map Info:
Data Exclusion: 3.00 σ
Points Excluded: 0
Points Selected: 49 out of 49
Max: 29.76 nm
Min: 27.44 nm
Range: 2.32 nm
Mean: 28.60 nm
StdD / %StdD: 0.73 nm / 2.54%
%NonU: 4.06%
Interval / %Intvl: 0.29 nm / 1.02%

(b)
Map Info:
Data Exclusion: 3.00 σ
Points Excluded: 0
Points Selected: 49 out of 49
Max: 29.76 nm
Min: 27.57 nm
Range: 2.19 nm
Mean: 28.67 nm
StdD / %StdD: 0.69 nm / 2.41%
%NonU: 3.82%
Interval / %Intvl: 0.27 nm / 0.96%

(c)
Map Info:
Data Exclusion: 3.00 σ
Points Excluded: 0
Points Selected: 49 out of 49
Max: 30.54 nm
Min: 28.19 nm
Range: 2.34 nm
Mean: 29.38 nm
StdD / %StdD: 0.77 nm / 2.62%
%NonU: 3.99%
Interval / %Intvl: 0.29 nm / 1.00%

(d)
Map Info:
Data Exclusion: 3.00 σ
Points Excluded: 0
Points Selected: 49 out of 49
Max: 0.1955
Min: 0.1909
Range: 0.0046
Mean: 0.1924
StdD / %StdD: 0.0012 / 0.62%
%NonU: 1.21%
Interval / %Intvl: 0.0006 / 0.30%

(e)
Map Info:
Data Exclusion: 3.00 σ
Points Excluded: 0
Points Selected: 49 out of 49
Max: 0.2965
Min: 0.2873
Range: 0.0093
Mean: 0.2907
StdD / %StdD: 0.0025 / 0.87%
%NonU: 1.60%
Interval / %Intvl: 0.0012 / 0.40%

(f)
Map Info:
Data Exclusion: 3.00 σ
Points Excluded: 0
Points Selected: 49 out of 49
Max: 0.3984
Min: 0.3884
Range: 0.0099
Mean: 0.3921
StdD / %StdD: 0.0029 / 0.75%
%NonU: 1.27%
Interval / %Intvl: 0.0012 / 0.32%

Figure 1.3: 49 points polar maps, with 6 mm edge exclusions, of the thickness **(a-c)** and Ge concentration **(d-f)** in 30 nm thick SiGe layers, with 20 %, 30 % and 40 % Ge, grown on Si(001) substrates.

The mean thickness obtained by SE is 15 to 20 Å below the mean thickness from XRR (**Tab. 1.2**). This can be explained by two reasons. First, XRR maps have been acquired with a 20 mm edge exclusion. Therefore, thicknesses close to the wafer edges were not taken into account when calculating the mean thickness, at variance with SE, with 24 points out the 49 points 6 mm away only from the wafer edges (**Fig. 1.3 (a-c)**). The native oxide thickness given by SE was always around 10 Å. Such values are higher than expected in reality which might lead to an underestimation of the SiGe layers thicknesses by a few angstroms. In addition, minimum and maximum values calculated from SE mappings are spread over 20 Å, which is not negligible at first sight. However, for subsequent experiments conducted in the central area of the wafer (with a 30 mm edge exclusion), the thickness dispersion should be divided by a factor of 2. In addition, from a relative point of view, thickness values obtained by SE are highly reproducible from a wafer to another.

The Ge concentrations measured by SE show a low dispersion (<1 %) with values close to the ones calculated from XRD measurements (1-1.5 %). The 3 wafers can be therefore considered as highly uniform from the Ge content perspective.

	Thickness (Å): $\begin{cases}\textbf{Max.}\\ \textbf{Min.}\\ \textbf{Mean}\end{cases}$		**Ge content (%):** $\begin{cases}\textbf{Max.}\\ \textbf{Min.}\\ \textbf{Mean}\end{cases}$	
Sample	**SE**	**XRR**	**SE**	**XRD**
SiGe 20 %	297.6 274.4 **286.0 ± 2.5 %**	310 301 **307.0 ± 0.9 %**	19.55 19.09 **19.24 ± 0.6 %**	- - **20.6 ± 1.0 %**
SiGe 30 %	297.6 275.7 **286.7 ± 2.4 %**	306 296 **302.9 ± 1.1 %**	29.65 28.73 **29.07 ± 0.9 %**	- - **30.4 ± 1.0 %**
SiGe 40 %	305.4 281.9 **293.8 ± 2.6 %**	312 301 **309.1 ± 1.1 %**	39.84 38.84 **39.21 ± 0.7 %**	- - **40.6 ± 1.0 %**

Table 1.2: (left) SiGe thicknesses from XRR (9 points polar maps at 0 cm, 7 cm and 13 cm from wafer centres) and from SE (49 points polar maps with 6 mm edge exclusions only). (Right) Ge contents from SE (49 points polar maps with 6 mm edge exclusions only) and from XRD (at the wafer centers).

1.3 Chemical analysis (ToF-SIMS, STEM-EDX)

For chemical analysis, two methods were used: time of flight secondary ion mass spectrometry (ToF-SIMS) and energy-dispersive x-ray spectroscopy assisted by scanning transmission electron microscopy (STEM-EDX). The former was performed at CEA-Leti and the latter at LAAS-CNRS.

Secondary Ion Mass Spectrometry measurements

The ToF-SIMS characterization method slightly differs from the conventional SIMS method, as it requires two primary ion beams: a low-energy ion beam for sputtering (0.1 – 2 keV) and a high-energy ion beam for the analysis (15 – 25 keV). Thanks to the low-energy ion beam, the early measurement transient discrepancies can be lowered. As the sputtering occurs slowly, better resolutions are reachable, as well. On the other side, the high-energy ion beam generates ions are analyzed in a free flight chamber instead of a mass spectrometer. As the free flight duration depends mainly on the mass, more species can be simultaneously analysed. For results thereafter, the sputtering was performed with O or Cs ions, while the analysis was made with Bi ions **[1]**. The typical widths of the sputtered and analysed areas were 250 µm and 70 µm, respectively.

Corrected and quantified depth profiles are shown in **Fig. 1.4**. All profiles exhibited artefacts in the first five nanometres below the surface that are associated to the early stages of the sputtering process. This transient measurement phenomenon has been removed from initial profiles. Excluding these effects and taking into account a ~2 % error on germanium content, the obtained depth profiles corroborate previous XRD, XRR and SE results, displaying SiGe layers with uniform composition at 20 %, 30 % and 40 % with thicknesses around 30 nm (when placing the SiGe/Si interface at half-height of the Ge profile tails). The thickness difference might come from uncertainties in the sputtering rate calibration procedure.

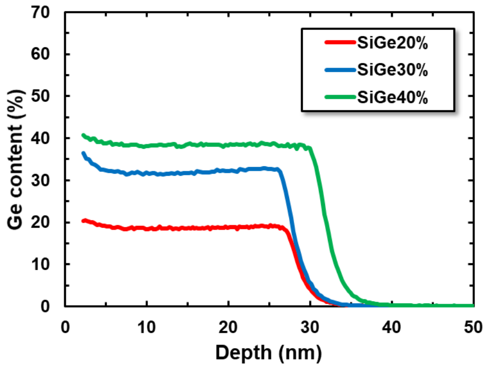

Figure 1.4: Corrected Ge concentration profiles as a function of depth in 30 nm-thick SiGe layers with 20 %, 30 % and 40 % of Ge, measured by ToF-SIMS.

Scanning Transmission Electron Microscopy combined with Energy-Dispersive x-ray (STEM-EDX) spectroscopy measurements

The scanning transmission electron microscopy (STEM) is a derivative mode of the conventional transmission electron microscopy (TEM) in which the electron beam is focused on a single point (~1 Å diameter) on the sample surface, forming a probe that scans the whole sample. The electron beam excites atoms inside the sample, which subsequently emit x-rays during their de-excitation. Energy-dispersive x-ray spectroscopy analysis consists in collecting these x-rays with dedicated detectors (**Fig. 1.5**). As these x-rays are characteristic of the energy levels of the emitting atom, some chemical information about the observed region of the sample can be obtained. Germanium maps and depth profiles of the atomic species were extracted from the collected data.

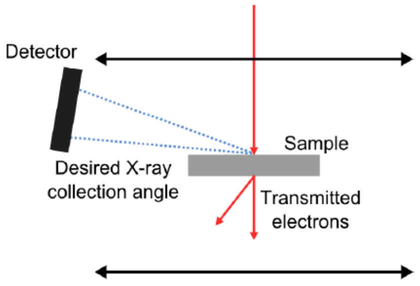

Figure 1.5: X-ray detection configuration for EDX observations in a TEM tool.

Long acquisition times are needed to improve the signal over noise ratio, but are limited by the induced damage on the TEM lamella and by the sample drift. For the results shown here, typical acquisition times of ~20 minutes were used for each sample. Data (x-ray counts) are then transformed into at.% values thanks to a quantification procedure based on the Cliff-Lorimer method. The resulting depth profiles are shown in **Fig. 1.6**. Variations in the Ge plateaux are attributed to measurement noise. Indeed, compared to ToF-SIMS measurements, where the sputtered areas are in the µm scale, the analysed area in STEM-EDX is significantly smaller (nm-scale). Therefore, final results are more impacted by local concentration variations inside the layer. Despite these variations, the same conclusions as in the case of ToF-SIMS can be drawn concerning the Ge concentration profiles.

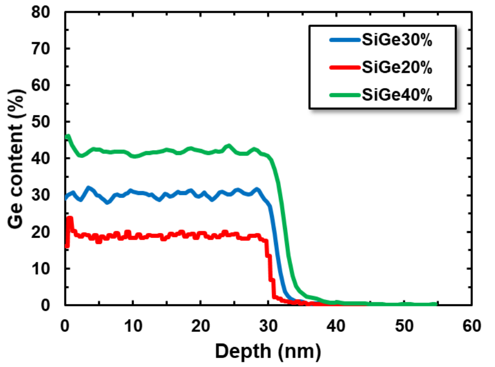

Figure 1.6: Ge concentration profiles as a function of depth of 30 nm-thick SiGe layers with 20 %, 30 % and 40 % of Ge from STEM-EDX.

1.4 Strain and defect characterizations and analysis (HRXRD, HRTEM)

Previous sections confirmed that the fabricated layers are in accordance with the nominal specifications in terms of Ge concentrations and layer thickness (mean values and uniformity). Additionally, the strain level in the grown layer was also investigated. Indeed, unwanted strain relaxation may lead to the appearance of crystal defects in the layer. To do so, two characterization techniques were used: high-resolution XRD reciprocal space mapping (RSM) (global analysis) and high-resolution TEM (local analysis).

Reciprocal Space Maps (RSM) by High-Resolution X-Ray Diffractometry (HRXRD)

RSMs around the (224) x-ray diffraction order were used to evaluate the strain inside the as-grown layers. Indeed, such an asymmetric measurement enables to determine the perpendicular and parallel lattice parameters ($a^{\perp}$ and $a^{\parallel}$, respectively) with respect to the surface. Acquisition times of 30 minutes were used to obtain acceptable signal over noise ratios. The resulting RSMs are displayed in **Fig. 1.7**. For all maps, the intense red spot in the upper part of the scan (star-shaped peak) corresponds to the bulk Si substrate while the second most intense peak (stripe-shaped red peak), corresponds to the SiGe epilayer. Both peaks are vertically aligned for each Ge concentration, meaning that all layers are fully compressively strained (i.e. pseudomorphic). Also, as expected, the distance between the Si peak (Q_z~4.62 nm^{-1}) and the SiGe peak (Q_z ~4.57 nm^{-1} at 20 %, Q_z ~4.54 nm^{-1} at 30 % and Q_z ~4.51 nm^{-1} at 40 %) linearly increases with the Ge concentration. Finally, the presence of sharp fringes around the SiGe peak is another indication of good uniformity in terms of Ge content, strain, layer thickness and surface/interface smoothness/abruptness. This phenomenon was also clearly seen in omega-2theta curves (**Fig. 1.2**).

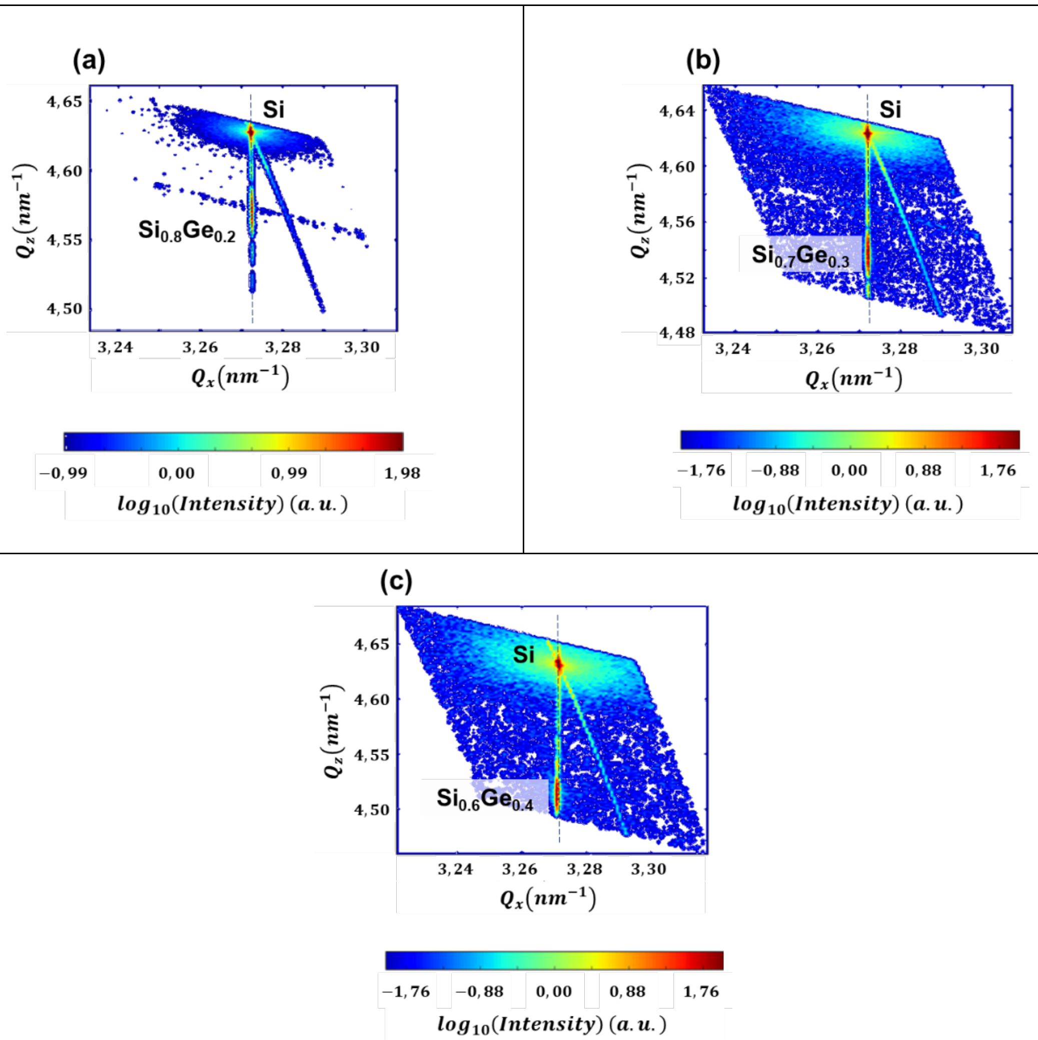

Figure 1.7: Reciprocal Space Maps along the (224) XRD order on 30 nm-thick SiGe layers with 20 % **(a)**, 30 % **(b)** and 40 % **(c)** of Ge.

High-Resolution Transmission Electron Microscopy (HRTEM)

Cross-section lamellas were prepared for TEM observations. In **Fig. 1.8**, we show a typical HR-TEM image from the $Si_{0.7}Ge_{0.3}$ layer on top of bulk Si. No apparent defects can be distinguished and the lattice matching at the Si/SiGe interface seems flawless. Other local inspections gave the same results.

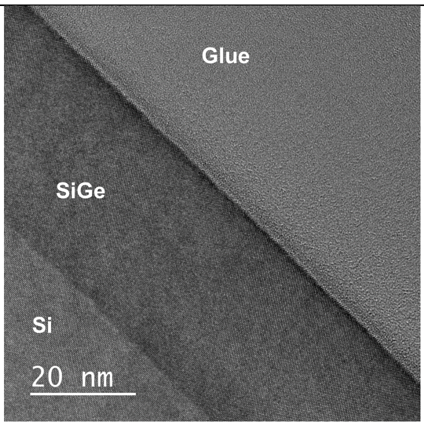

Figure 1.8: HR-TEM cross-section image of the 30 nm thick SiGe layer with 30 % of Ge.

In summary, the extended characterization results shown in this section indicate that the SiGe layers fabricated at CEA-Leti exhibit a very good uniformity in thickness and Ge concentration over the entire wafer surface (300 mm wafers). Grown layers are perfectly strained (compressive), with no evidence of defects at the Si/SiGe interface or inside the epilayer. The perfect correspondence between the nominal and the effective wafer characteristics was also confirmed for all other undoped SiGe wafers from the same batch of samples (cf. D3.2, Fig. 1).

2 Doped SiGe epi-layers

Strained SiGe alloy layers are typically used for the fabrication of PMOS source/drain modules and the usual dopant is boron. In order to fulfil the IRDS resistance and contact resistivity requirements, boron doping concentrations must be in the order of $1x10^{20}$ cm^{-3}. In order to properly investigate the *in-situ* doping process and the impact of subsequent annealing processes on the final dopant electrical activation, while limiting the total number of fabricated wafers, it was decided to fix the Ge content in the SiGe layer for this study (30 at. %) and select three different boron doping concentration around the reference $1x10^{20}$ cm^{-3} level.

2.1 Fabrication process

As well as for undoped SiGe layers and based on existing data points, a few SiGe30%:B growth trials were performed on Si:P capped Si(001) 300 mm wafers **[3]**. The main goal of these tests was to optimize the growth duration, the lamp power ratio and the species flows to obtain 30 nm-thick SiGe30%:B layers with the desired doping levels and the best layer uniformity possible. Based on these preliminary tests, a growth condition was identified that yielded a boron concentration of ~$1.5x10^{20}$ cm^{-3}. Growth conditions were subsequently modified compared to that reference in order to obtain two additional recipes yielding boron concentrations respectively below and above ~$1.5x10^{20}$ cm^{-3}.

In practice, a deposition of an in-situ phosphorous-doped Si layer (10^{19} cm^{-3}) was first performed at 950 °C, 10 Torr with a $SiH_2Cl_2/PH_3/HCl$ chemistry on 300 mm low p-type Si(001) substrates. Then, a HF/SC1 wet cleaning was carried out to remove the native oxide (together with residual P atoms on the surface) and form a chemical oxide. A Siconi surface preparation chamber was then used to transform the chemical oxide into salts before sublimating them at

180 °C. Finally, an H_2 bake at 850 °C for 2 minutes was used to get rid of the residual O contamination on the surface. Finally, the SiGe30%:B layers were deposited at 650 °C, 20 Torr with the same SiH_2Cl_2, GeH_4 and HCl flows and with various B_2H_6 flows to obtain the desired *in-situ* doping levels, named A (i.e. below ~$1.5x10^{20}$ cm^{-3}), B (~$1.5x10^{20}$ cm^{-3}) and C (i.e. above ~$1.5x10^{20}$ cm^{-3}).

2.2 Optical analysis (XRR, XRD, ES)

Same characterizations as for undoped SiGe layers (previous section) were conducted at CEA-Leti to determine the “apparent” Ge concentrations and the layer thicknesses: x-ray reflectivity (XRR), x-ray diffraction (XRD) and spectroscopic ellipsometry (SE).

X-Ray Reflectivity (XRR) measurements

The flatness of the surface and the abruptness of the SiGe/Si interfaces were confirmed by XRR measurements at the wafer centres. Indeed, curves in **Fig. 2.1** display clear fringes even at high incidence angles θ. No significant impact of doping on the wafer physical properties can be noticed.

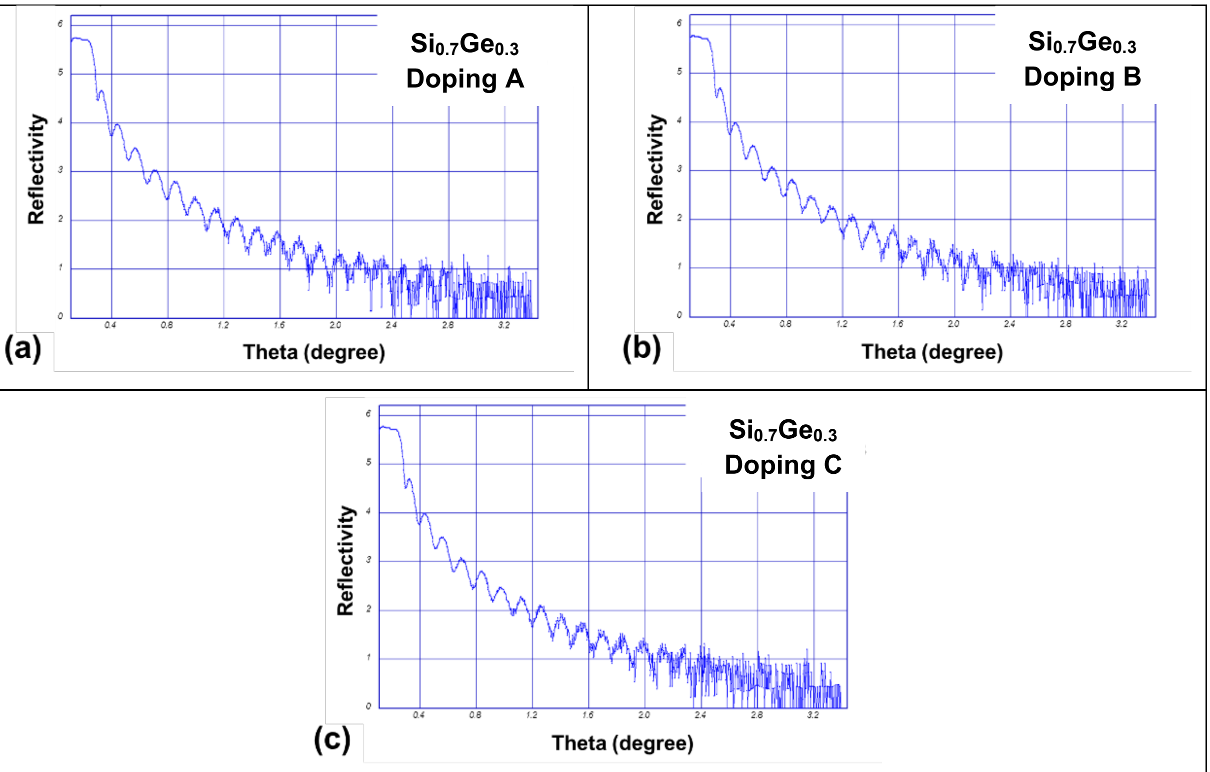

Figure 2.1: X-ray reflectivity curves for 30 nm thick SiGe30%:B layers grown on top of p-type Si(001) substrates capped with ~300 nm of Si:P (10^{19} cm^{-3}) and with various concentrations of boron. **(a)** sample A (< ~$1.5x10^{20}$ cm^{-3}); **(b)** sample B (~$1.5x10^{20}$ cm^{-3}); **(c)** sample C (> ~$1.5x10^{20}$ cm^{-3}).

The uniformity of the wafers was evaluated thanks to FFTs on 9 points polar maps’ XRR profiles (at 0 cm, 7 cm and 13 cm from the wafer centers). Calculated thicknesses are summarized in **Tab. 2.1** and show an excellent reproducibility with average thicknesses of 29.3 nm, 30.2 nm and 30.3 nm for boron-doped SiGe30% at levels A, B and C, respectively.

Doping level	Mean thickness (Å)			Overall mean thickness (Å)
	At 0 cm	At 7 cm	At 13 cm	
A (< ~1.5x10^{20} cm^{-3})	295.0 ± 0.3 %	296.0 ± 0.3 %	289.0 ± 0.1 %	**292.8 ± 1.2 %**
B (~1.5x10^{20} cm^{-3})	300.0 ± 0.3 %	303.5 ± 0.3 %	301.2 ± 0.2 %	**302.1 ± 0.5 %**
C (> ~1.5x10^{20} cm^{-3})	301.0 ± 0.2 %	305.5 ± 0.2 %	301.0 ± 0.1 %	**303.0 ± 0.8 %**

Table 2.1: Calculated thicknesses obtained after applying FFT on XRR profiles (9 points polar maps at 0 cm, 7 cm and 13 cm from the wafer centers).

X-ray Diffractometry analysis

Omega-2theta scans around the (004) x-ray diffraction (XRD) order were performed to confirm the apparent amount of Ge and the thicknesses of the SiGe:B layers. **Fig. 2.2** curves show well-defined and intense bulk Si peaks at 0 arcsec and SiGe layer peaks with thickness fringes on both sides. Calculated thickness and Ge concentrations (simulations based on dynamical diffraction theory) are: 29.5 nm (32.7 % Ge), 30.0 nm (31.6 % Ge) and 30.1 nm (29.8 % Ge) for SiGe:B doping at levels A, B and C, respectively (assuming a ~2 % error on germanium content and a 1 nm error on the depth resolution). Thickness results are in good agreement with XRR results. Concerning Ge concentrations, the lowest doped layer is slightly above the target (32.7 %), but only a measurement at the centre of the wafer was performed in that case. The good uniformity will be discussed later, based on SE measurement. What can be noticed however, is that the so-called “apparent” Ge concentration slightly decreases as the doping level increases. This is due to compressive strain compensation by boron atoms, whose radius (a_B = 3.78 Å) is much smaller than Si and Ge atoms (a_{Si} = 5.431 Å and a_{Ge} = 5.658 Å). The measured Ge content is therefore artificially lowered by this phenomenon.

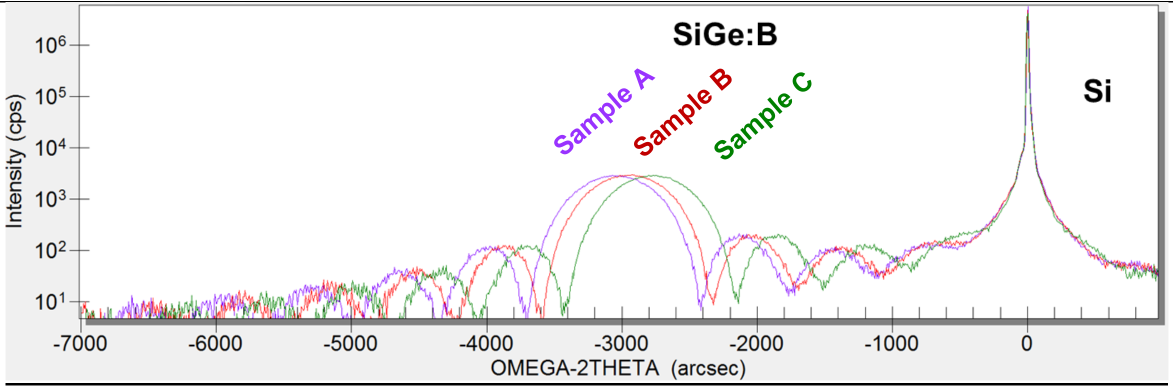

Figure 2.2: Omega-2Theta scans around the (004) XRD order on 30 nm thick SiGe30%:B layers with different doping levels (A, B and C, see text) on Si(001) substrates. The well-defined, intense SiGe:B layer peaks with thickness fringes on both sides move towards the Si substrate peak as the substitutional boron concentration increases (compressive strain compensation by small size boron atoms).

Spectroscopic Ellipsometry measurements

Layer thickness and Ge concentration uniformity monitoring was performed by spectroscopic ellipsometry. 49 points polar maps with 6 mm edge exclusions were acquired on the lowest doped SiGe30% layer (sample A). Simulations yielded layer thicknesses (**Fig. 2.3 (a)**) and Ge concentration (**Fig. 2.3 (b)**) maps.

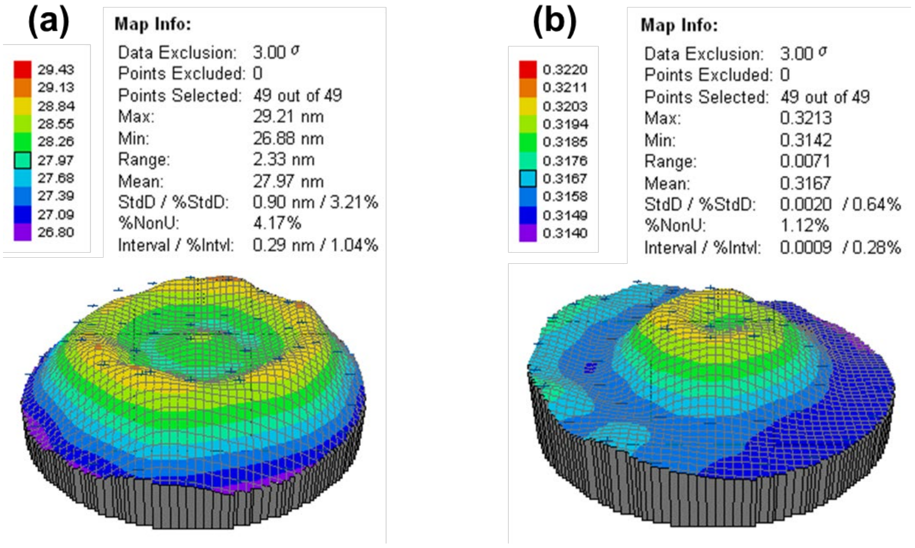

(a)

Map Info:

Data Exclusion: 3.00 σ
Points Excluded: 0
Points Selected: 49 out of 49
Max: 29.21 nm
Min: 26.88 nm
Range: 2.33 nm
Mean: 27.97 nm
StdD / %StdD: 0.90 nm / 3.21%
%NonU: 4.17%
Interval / %Intvl: 0.29 nm / 1.04%

(b)

Map Info:

Data Exclusion: 3.00 σ
Points Excluded: 0
Points Selected: 49 out of 49
Max: 0.3213
Min: 0.3142
Range: 0.0071
Mean: 0.3167
StdD / %StdD: 0.0020 / 0.64%
%NonU: 1.12%
Interval / %Intvl: 0.0009 / 0.28%

Figure 2.3: 49 points polar maps, with 6 mm edge exclusions, of the thickness **(a)** and Ge concentration **(b)** in a 30 nm thick SiGe30%:B cm^{-3} layer on a Si(001) substrate with the lowest doping concentration (sample A, < ~1.5x10^{20} cm^{-3}).

The thicknesses and Ge contents measured with the three techniques (SE, XRR and XRD) in the lowest B concentration sample (e.g. in sample A) are summarised in Table 2.2. The mean thickness obtained by SE is 15 Å below the mean thickness measured by XRR. This can be explained by the same reasons cited in previous section: smaller edge exclusion for SE measurements (6 mm) than for XRR measurements (20 mm) and the presence of thin native oxide (~10 Å) that results in smaller SiGe layer thickness in SE than in XRR. Concerning the Ge concentration results, calculated values show a remarkably low dispersion (<1 %) with values close to that from XRD (<1 %). The measured layer can therefore be considered as being highly uniform in terms of Ge content.

	Thickness (Å): $\left\{\begin{array}{l}\textbf{Max.}\\\textbf{Min.}\\\textbf{Mean}\end{array}\right.$		**Ge content (%):** $\left\{\begin{array}{l}\textbf{Max.}\\\textbf{Min.}\\\textbf{Mean}\end{array}\right.$	
Sample	**SE**	**XRR**	**SE**	**XRD**
A (< ~5x10^{20} cm^{-3})	292.1 268.8 **279.7 ± 3.2 %**	296 289 **292.8 ± 1.2 %**	32.13 31.42 **31.67 ± 0.6 %**	- - **32.7 ± 1.0 %**
B (~1.5x10^{20} cm^{-3}**)**	- - **-**	300 304 **302.1 ± 0.5 %**	- - **-**	- - **31.6 ± 1.0 %**
C (> ~1.5x10^{20} cm^{-3}**)**	- - **-**	301 306 **303.0 ± 0.8 %**	- - **-**	- - **29.8 ± 1.0 %**

Table 2.2: (left) SiGe thicknesses from XRR (9 points polar maps at 0 cm, 7 cm and 13 cm from wafer centres) and from SE (49 points polar maps with 6 mm edge exclusions only). (Right) Ge contents from SE (49 points polar maps with 6 mm edge exclusions only) and from XRD (at the wafer centers).

2.3 Chemical analysis (SIMS)

Chemical analysis by Secondary Ion Mass Spectrometry (SIMS) on the B-doped SiGe layers were performed at Ł-IMiF.

SIMS measurements were performed with the CAMECA IMS SC Ultra instrument. Cs+ ions with ultra-low impact energy (100 eV) were used as a primary beam. The incident angle was 75°. As a result, the depth resolution was below 1 nm, resulting in a very precise characterization of the surface and interface.

For such non-trivial conditions (particularly high incident angle), most of the primary ions are reflected from the sample and only about one out of a thousand primary ions is able to sputter atoms out from the surface of a sample. Under such conditions, the matrix effect which typically hinders the quantification of SIMS results is strongly reduced or even eliminated.

In all experiments, a positive detector polarity was used and thus signals were registered as CsX+ complex ions. Germanium and silicon concentrations were calibrated independently, based on CsGe+ and CsSi+ signals, respectively. To determine B concentration, a complex ion CsSi2B+ was normalized point-to-point to CsSi2+ signal. A series of reference samples with known compositions and B concentrations was used.

Quantification of germanium and boron concentration was excellent with such SIMS protocols. Uncertainties were 0.57 % and 1.92 % for Ge and B concentrations, respectively, while the depth resolution was 0.6 nm/decade.

Germanium and boron profiles are shown in **Fig. 2.4**. The average germanium concentration is 29.8 ± 1.0 at. % in the three samples. Assuming a 1-2 % error is introduced during SIMS profile conversion, obtained values are in good agreement with the nominal value. This also confirms that the apparent decrease of the Ge concentration observed in XRD when the doping level increases (cf. Fig. 2.2) is indeed due to compressive strain compensation. Ge and B profiles exhibit a sharp concentration decrease around 30 nm, suggesting that the

SiGe:B/Si interface is perfectly uniform. This was confirmed by TEM analyses (not shown), which were all similar to the one shown in **Fig. 1.8**. As for the boron concentration profiles, a sharp B pile-up (with concentration exceeding 1x10^{21} cm^{-3}) is observed at the SiGe surface. Several SIMS measurements and quantification procedures were performed, confirming that those pile-ups were not measurement artefacts. However, such pile-ups are no longer observed in samples submitted to subsequent annealing steps.

Finally, SIMS measurements enabled a precise measurement of the boron concentration in the three doped layers. The average boron concentration in the sample fabricated using the reference process (sample B) was (1.425 +/- 0.027) x 10^{20} atoms/cm^3, in perfect agreement with the expected value (~1.5x10^{20} cm^{-3}). As for the other samples, an average boron concentration of (7.37 +/- 0.14) x 10^{19} atoms/cm^3 was measured in the "lowly doped" sample (sample A), while a concentration of (2.334 +/- 0.046) x 10^{20} atoms/cm^3 was obtained in the highest doping concentration sample (sample C).

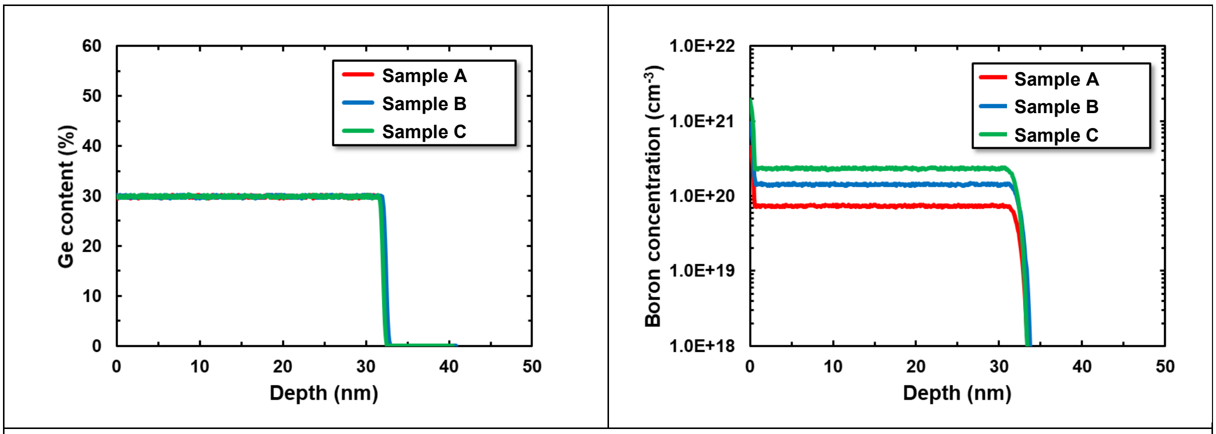

Figure 2.4: Germanium **(a)** and boron **(b)** concentration profiles as a function of depth obtained by SIMS for 30 nm-thick *in-situ* boron-doped $Si_{0.7}Ge_{0.3}$ layers at different boron concentration levels: 7.4x10^{19} cm^{-3} (sample A, red); 1.4x10^{20} cm^{-3} (sample B, blue); 2.3x10^{20} cm^{-3} (sample C, green).

2.4 Strain and defect characterizations and analysis (HRXRD)

Reciprocal space maps were acquired to assess the strain inside the boron-doped SiGe layers. Maps are displayed in **Fig. 2.5**. As in the previous section, two main peaks are present in each RSM: an intense round peak corresponding to bulk Si (Q(z)~4.62 nm^{-1}) and an intense elongated peak associated to SiGe layers (Q(z)~4.55 nm^{-1}). Both peaks are vertically aligned for all 3 wafers, indicating that all SiGe layers are fully strained in compression. The good uniformity in both Ge content and strain level in the whole layer thickness are evidenced by the presence of clear fringes around the SiGe peak.

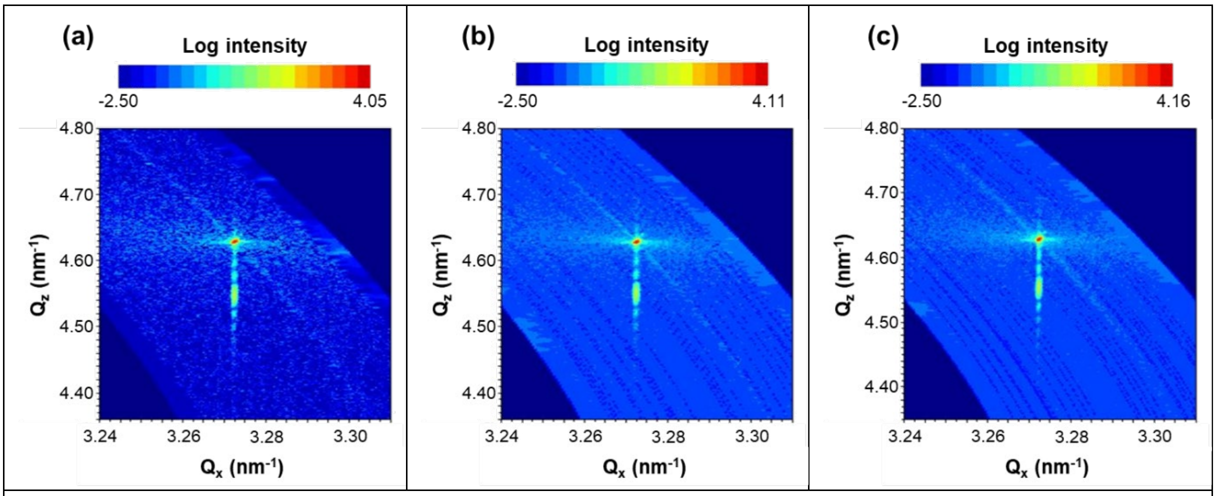

Figure 2.5: Reciprocal space maps along the (224) direction obtained by HR-XRD of 30 nm-thick *in-situ* boron-doped $Si_{0.7}Ge_{0.3}$ layers with different boron concentrations: **(a)** sample A (7.4x10^{19} cm^{-3}); **(b)** sample B (1.4x10^{20} cm^{-3}); **(c)** sample C (2.3x10^{20} cm^{-3}).

2.5 Boron activation analysis (Hall effect)

In order to have a first evaluation of the doping level inside the SiGe:B layers, 4PP measurements were conducted at CEA-Leti. However, in the case of thin doped layers such as those investigated here, this method is highly sensitive to probe depth penetration and therefore on the probe characteristics (i.e. the curvature radius of the probe tips). Indeed, results with 2 different sets of probes were not reproducible, although a clear decrease of the sheet resistance when increasing the boron doping concentration was observed in both cases. Consequently, the results were not exploited for a quantitative analysis of the electrical activation of these layers. For this reason, further investigations were carried out by combining Hall-effect measurements (at CNRS-LAAS) and SIMS profiles (Ł-IMiF).

Van der Pauw structures (cross and square) were fabricated on pieces from each wafer and measured by Hall effect. Typical injected currents of 1µA to 1mA and a magnetic field of 0.3 T were used. Multiple sets of measurements were conducted to confirm the good reproducibility of the results. Extracted sheet resistances R_S, Hall doses N_H and Hall mobilities μ_H are summarized in **Tab. 2.3 (blue data)**. Hall doses and mobilities were converted into real doses N and mobilities µ assuming a scattering factor of r_H~0.35 for SiGe30% **Tab. 2.3 (black data) [4-7]**. Similarly to 4PP measurements, the increase of the active Hall dose with the boron concentration qualitatively confirms the improvement of the activation level. However, in the case of the sample doped with the highest boron concentration (2.3x10^{20} cm^{-3}), it is obvious that the measured active dose (4.66x10^{14} cm^{-2}) is much lower than the chemical boron dose from SIMS (~6.9x10^{14} cm^{-2}), indicating that a large fraction of the boron atoms is not electrically active. Further analysis had therefore to be carried out to quantify the activation rate. This was achieved by comparing the Hall electrical measurements with Hall parameters calculated from boron SIMS profiles (**Eq. 1-3**).

		SiGe30%		
	Sample name	**A**	**B**	**C**
	Boron conc. (cm^{-3})	**$7.4\text{x}10^{19}$**	**$1.4\text{x}10^{20}$**	**$2.3\text{x}10^{20}$**
Hall effect measurements (r_H~0.35)	**Rs (Ω/sq)**	383	261	215
	N_H (cm^{-2})	$6.57 \text{ x } 10^{14}$	$1.03 \text{ x } 10^{15}$	$1.33 \text{ x } 10^{15}$
	N (cm^{-2})	$2.30 \text{ x } 10^{14}$	$3.62 \text{ x } 10^{14}$	$4.66 \text{ x } 10^{14}$
	μ_H (cm^2/(V.s))	25	23	22
	μ (cm^2/(V.s))	71.4	66.0	62.8

Table 2.3: Sheet resistance R_s, Hall dose N_H and Hall mobility μ_H measured by Hall effect on 30 nm-thick in-situ boron-doped $Si_{0.7}Ge_{0.3}$ layers with different boron concentrations.

To evaluate the partial activation level of any doped layer, a uniform active doping level n_{elec} was fixed and applied as a filter to the boron SIMS profile **[8,9]**. Due to the high quality of the CVD fabrication process, the assumption of a uniform active doping level is most likely close to reality, whether it is fully activated or not. From the filtered SIMS profile, the Hall dose is calculated thanks to the following formula and compared to the electrical one. The active doping level n_{elec} is tuned until both calculated and measured Hall doses match (r_H~0.35).

$$N_{H_{calc}} = \frac{\left[\int_0^d n_{elec}(z)\langle\mu(z)\rangle dz\right]^2}{r_H \int_0^d n_{elec}(z)\langle\mu^2(z)\rangle dz} \qquad \textbf{(1)}$$

Once the maximum active doping level, n_{elec}, is determined, the other parameters measured by the Hall technique can be calculated according to the following formulas:

$$R_{S_{calc}} = \frac{1}{\alpha q \int_0^d n_{elec}(z)\langle\mu(z)\rangle dz} \qquad \textbf{(2)}$$

$$\mu_{H_{calc}} = \frac{\alpha r_H \int_0^d n_{elec}(z)\langle\mu^2(z)\rangle dz}{\int_0^d n_{elec}(z)\langle\mu(z)\rangle dz} \qquad \textbf{(3)}$$

with:

$$\mu(z) = \mu(n(z)) = \mu_0 e^{-\frac{p_c}{n(z)}} + \frac{\mu_{max}}{1 + \left(\frac{n(z)}{C_r}\right)^{\alpha}} - \frac{\mu_1}{1 + \left(\frac{C_s}{n(z)}\right)^{\beta}}$$

and the different coefficient values: $\mu_1 = 29,\ \alpha = 29,\ \beta = 2,\ \delta = 1,\ C_r = 2.23 \times 10^{17},\ C_s = 6.10 \times 10^{20},\ p_c = 9.23 \times 10^{16}$

x_{Ge}	**0**	**0.1**	**0.2**	**0.3**	**0.4**	**1.0**
μ_0	44.9	45	50.6	60	69	69
μ_{max}	470.5	409.8	506.3	630.9	792	792

Here, the α parameter is a mobility degradation factor ($\alpha \leq 1$), which is introduced to account for the possible impact of the inactive dopant fraction on the carrier transport mechanism. In the case of a full dopant activation (or when the electrically inactive dopants do not degrade the carrier mobility), α is equal to unity.

This method was first applied starting from the raw boron SIMS profiles of the three boron-doped SiGe layers shown in Fig 2.4(b) and reproduced in **Fig. 2.6 (a)**. The extracted parameters are summarized in **Tab. 2.3 (blue data)**. The obtained maximum doping level, n_{elec}, for the lowly-doped layer (sample A) corresponds (within the experimental errors) to the boron plateau concentration measured by SIMS (7.4×10^{19} cm^{-3}), leading to an almost complete activation rate, Ω, of 92.8 % and undeteriorated carrier transport properties (α=1). For moderately and highly doped SiGe layers, the active concentrations are below the measured boron plateaus. Thus, the layers are partially activated at 75 % and 58 %, respectively. We can also observe a slight decrease of the α factor when increasing the *in-situ* doping level (α=0.99 and α=0.97, respectively). Such small variations compared to unity are lower than experimental uncertainties associated to SIMS and Hall-effect measurements. We can therefore conclude that the electrical transport degradation is absent or negligible even in the highly doped sample, where only ~60 % of the boron atoms are electrically active. This result strongly differs from the case of electrically inactive boron introduced by ion implantation, where the formation of relatively large boron-interstitial clusters may induce a strong carrier mobility degradation (α~0.6) **[10]**.

		SiGe30%		
	Sample name	**A**	**B**	**C**
	Boron conc. (cm^{-3})	**7.4×10^{19}**	**1.4×10^{20}**	**2.3×10^{20}**
Raw data (Fig. 2.6 (a))	**n_{elec} (cm^{-3})**	7.18×10^{19}	1.12×10^{20}	1.44×10^{20}
	α (-)	1	0.99	0.97
	Ω (%)	**92.8**	**75.1**	**58.3**
Filtered data (Fig. 2.6 (b))	**n_{elec} (cm^{-3})**	7.18×10^{19}	1.12×10^{20}	1.44×10^{20}
	α (-)	1	0.99	0.97
	Ω(filtered) (%)	**97.4**	**79.1**	**62.3**
Cut data (Fig. 2.6 (c))	**n_{elec} (cm^{-3})**	7.40×10^{19}	1.14×10^{20}	1.47×10^{20}
	α (-)	1	0.99	0.97
	Ω (%)	**99.3**	**80.6**	**63.7**

Table 2.3: Electrical level n_{elec}, mobility degradation factor α and activation rate Ω, calculated from the comparison between original and modified boron SIMS profiles (displayed in **Fig. 2.6**) and electrical parameters measured by Hall effect on 30 nm-thick in-situ boron-doped $Si_{0.7}Ge_{0.3}$ layers with different boron concentrations.

In order to estimate the impact of the boron pile-up measured by SIMS at the SiGe surface on the boron activation rate, Ω, the same calculations were performed after slightly modifying the boron SIMS profiles (**Fig. 2.6 (b) and (c)**). Two modifications were implemented on the raw SIMS profiles: one in which the surface peak was replaced by a constant concentration equal to that of the plateau (**Fig. 2.6 (b)**) and another in which the surface peak was simply removed (**Fig. 2.6 (c)**). Results are shown in **Tab. 2.3 (green and purple data)**. They are named "filtered data" and "cut data" for the sake of clarity. For the "filtered" data, the activation level n_{elec} remains unchanged. However, replacing the surface peak by a lower constant value results in a reduction of the atomic B sheet concentration, which in turn increases the activation rate by around 4 % for all samples. However, the previous conclusions remain unchanged, i.e. the lowly doped SiGe layer is fully activated whereas the other layers are only partially activated. Again, the mobility degradation parameter α remains close to unity in all samples. For the "cut" data, the results exhibit the same behaviour for both α and Ω (the latter further increasing by 1-2 %, due to the reduced thickness of the doped layer).

In summary, modifying the original boron SIMS profile to determine the impact of the surface boron pile-up did not change the final results significantly (~5 %). For this reason, we confirm that, while the electrically active dose increases when increasing the boron doping level from $7.4\text{x}10^{19}$ cm^{-3} up to $2.3\text{x}10^{20}$ cm^{-3}, the activation rate correspondingly decreases from ~100 % down to ~80 % and ~60 % for lowly, medium and highly doped SiGe30% layers, respectively. However, even in the presence of high fractions of electrically inactive boron, carrier transport properties are not deteriorated compared to a fully activated doped layer.

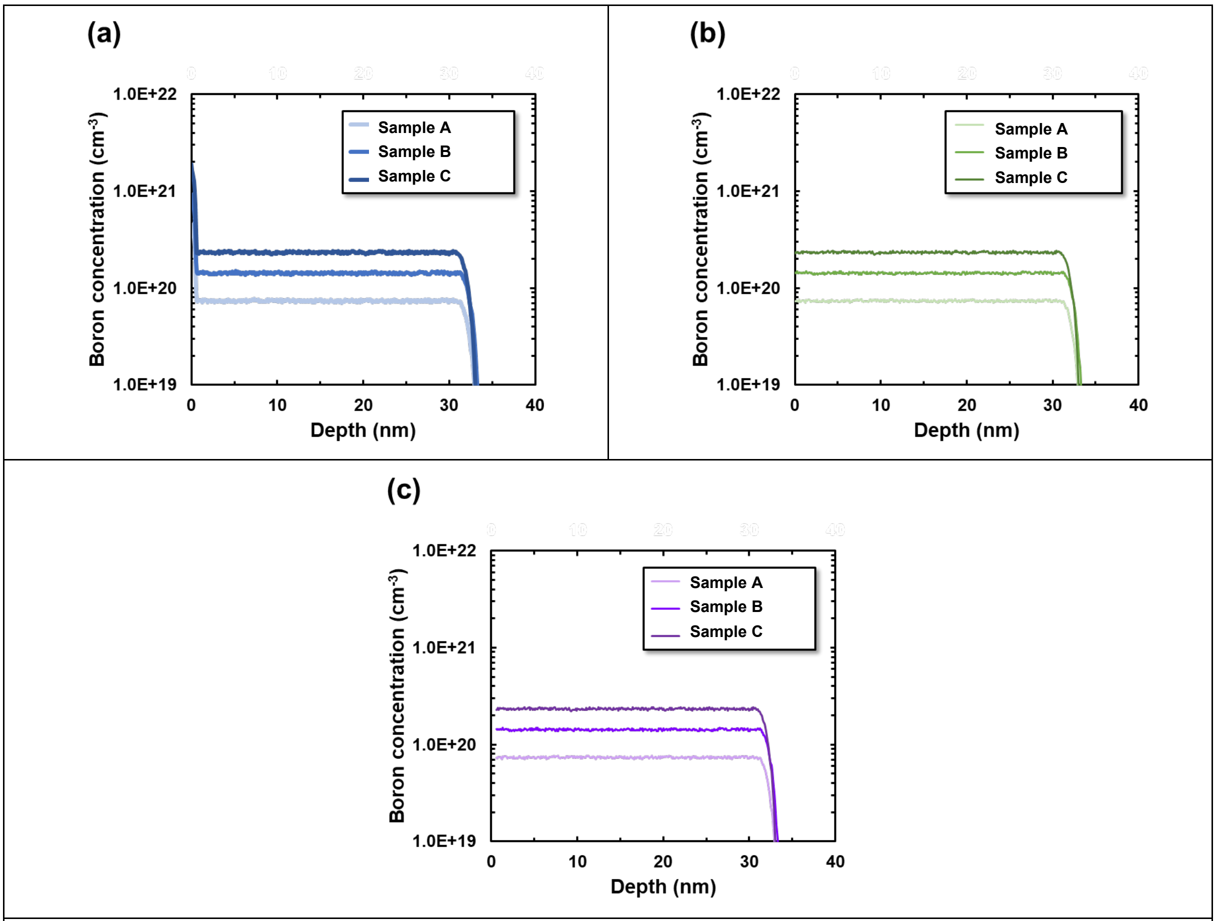

Figure 2.6: SIMS boron depth profiles in 30 nm-thick in-situ boron-doped $Si_{0.7}Ge_{0.3}$ layers with different boron concentrations from **(a)**. Original profiles **(b)** modified profiles obtained by replacing the surface peak by a constant value equal to that in the concentration plateau and **(c)** modified profiles obtained by removing the surface peak.

To conclude, we have demonstrated in this second section our ability to deposit compressively strained boron-doped SiGe layers on top of bulk Si by CVD with boron concentrations of: 7.0×10^{19} cm^{-3}, 1.3×10^{20} cm^{-3} and 2.3×10^{20} cm^{-3}. We have shown their good uniformity in terms of thickness, Ge concentration and strain over 300 mm wafers. By combining Hall-effect measurements and SIMS chemical profiles, we have shown their activation rates to be 100 %, 80 % and 60 %, respectively. Activation processes should therefore be used when using really large amounts of dopants in *in-situ* doped SiGe.

3 DoE on post-epitaxy anneals

Results shown in the previous sections indicate that it is possible to grow thin, perfectly strained and defect-free SiGe layers with different boron doping concentrations close to 1x10^{20} cm^{-3}. However, the boron activation rate was found to decrease when the atomic boron concentration increases. In order to improve such fabrication process, while gaining a deeper insight in the dopant activation mechanism, a new Design-of-Experiment (DoE) has been discussed and agreed within the consortium. Its aim is to increase the activation rate of as-grown layers by performing different post-epitaxy anneals.

In agreement with the overall objectives of the MUNDFAB project, only low thermal-budget annealing methods will be considered for this experiment. The first one is laser annealing. For the purpose of this experiment, laser annealing will be investigated only in submelt conditions. Indeed, laser-induced melt would result in a considerable redistribution of the Ge atoms during solidification, resulting in an irreversible modification of the starting material, which is out of the scope of this experiment. Alongside with laser annealing, low-temperature furnace annealing will also be investigated. In this case, the investigated temperature range might include values above 600 °C (but only for the sake of an improved understanding of the associated physical phenomena) and will serve as a reference process for the more complex laser annealing.

Available annealing tools

A wide range of annealing tools is available within the MUNDFAB consortium, including the Quantum Annealing (QA) tool, which is accessible through one of the Privileged partners (SCREEN-LASSE). The complete list of available tools is presented in **Tab. 3.1**. The different laser tools will enable to estimate the impact of various parameters on the dopant activation mechanisms. These will include the laser radiation nature (continuous vs pulsed), the laser wavelength, the pulse duration and pulse frequency rate. As mentioned above, the furnace annealing tool will provide reference data against which laser data will be compared.

Laboratory	**CNR-IMM Catania**	**CNR-IMM Padova (UNIPD)**	**SCREEN-LASSE**	**CEA-Leti**	**CEA-Leti or CNRS-LAAS**
Name	CW	COMPex 201F	QA	LT3100	Furnace
Anneal type	Continuous laser	Pulsed laser (excimer: KrF)	Pulsed laser (confidential)	Pulsed laser (excimer: XeCl)	
Wavelength	800 nm	248 nm	Confidential	308 nm	-
Pulse duration	-	21 ns	Confidential	160 ns	-
Frequency	-	0 – 10 Hz	High frequency	0 – 4 Hz	-
Shot size	~2x10 mm^2	5 x 5 mm²	20 x 20 mm²	18 x 18 mm²	-

Tab. 3.1: Available annealing tools for low-thermal budget post-epitaxy activation DoE.

Design of experiment (wafers and conditions)

In order to limit the total number of generated samples while enabling an exhaustive investigation of post-epitaxy dopant activation mechanisms, the experiment will be limited to two boron doping concentrations: the lowest one (7.4x10^{19} cm^{-3}) and the highest one (2.3x10^{20} cm^{-3}). The laser annealing tool available at CEA-Leti (LT3100) as well as the "reference" furnace anneals will be used to investigate both doping levels, while the laser annealing techniques available at other consortium sites will be tested only on the highly-doped layers, as summarised in **Tab. 3.2**.

		1	2	3	4	5	6	7
Doping								
SiGe 30 % (30nm) *in-situ* boron doping	7.4 x 10^{19} cm^{-3} **(Low)**	x					x	
	2.3 x 10^{20} cm^{-3} **(High)**		x	x	x	x		x
Annealing								
Laser annealing	LT3100 (CEA-Leti)	x	x					
	COMPex 201F (CNR-UNIPD)			x				
	CWL (CNR-IMM)				x			
	QA (SCREEN-LASSE)					x		
Furnace annealing	Furnace (CEA-Leti or CNRS-LAAS)						x	x

Tab. 3.2: Design of experiment to study the impact of different laser parameters, (namely the laser type, wavelength, pulse duration and pulse frequency) on the activation of boron in pseudomorphic *in-situ* boron-doped SiGe30% layers grown by CVD.

For each laser annealing technique, the melt threshold will first be determined from single-pulse tests (for pulsed laser) and duration tests (continuous laser). From these tests, about five energy density sub-melt conditions will be selected. For each energy density, several samples will be generated by changing the number of laser pulses. The estimated total number of samples generated with each tool is reported in the bottom line of **Tab. 3.3**, together with details on the corresponding experimental parameters.

Laboratory	**CNR-IMM**	**CNR-UNIPD**	**SCREEN**	**CEA-Leti**	**CEA-Leti or CNRS-LAAS**
Energy densities	-	4 cond. (< 0.60 J/cm²)	2 cond. (to determine)	3 cond. (< 1.45 J/cm²)	-
Number of pulses	-	4 cond. (1, 3, 30, 300 pulses)	5 cond. (to be determined)	8 cond. (1, 3, 10, 30, 100, 300, 1000, 10000 pulses)	-
Duration time	3 cond. (to be determined)	-	-	-	4 conditions/temperature
Temperature	-	-	-	-	500-800 °C
Total cond./wafer	**10**	**8**	**10**	**24**	**16**

Tab. 3.3: Planned number of conditions per wafer for each annealing technique.

Characterizations

Different parameters need to be measured to monitor the impact of sub-melt laser anneals on these layers: B and Ge chemical profiles, activation rate, crystalline quality, strain and roughness. To do so, several characterization methods will be used (**Tab. 3.4**). For boron and germanium chemical depth profiles, we will use the SIMS expertise of L-IMIF. Activation rate, further electrical properties (active dose and mobility) and active profiles will be measured by 4PP (CEA-Leti) and by Hall Effect/Differential hall Effect (CNRS-LAAS). The presence of crystalline defects or clusters will be investigated by TEM (CNRS-LAAS). Strain and Ge composition will be analysed by HRXRD (CEA-Leti). Finally, the surface roughness will be checked by AFM (CNRS-LAAS) and/or haze measurements (CEA-Leti).

Method	**SIMS**	**Hall Effect / 4PP**	**Differential Hall Effect (DHE)**	**TEM**	**XRD**	**AFM / Haze**
Parameter	B/Ge chem. profiles	Activation & electrical param.	Active profile	Cristal defects / clusters	Strain (& Ge composition)	Surface roughness
Operator (laboratory)	Ł-IMiF	LAAS / Leti	LAAS	LAAS	Leti	LAAS
Sample size requirement	5 x 5 mm²	5 x 5 mm²	16 x 16 mm²	10 x 10 mm² (less if FIB lam.)	5 x 5 mm²	< 2 x 2 mm²

Tab. 3.4: Planned characterizations along with corresponding measured parameters, samples size requirements and partner in charge.

Based on the size of the laser beam available in each laser tool, all of the characterization techniques reported in the table above can be performed with no particular limitation, the only exception being Differential Hall effect (DHE), which requires a minimum irradiated area of 15x15 mm^2. Such large surface will only be available at CEA-Leti (LT3100) and Lasse Screen (QA). More generally, in the case of small laser beams (COMPex 201F, 5 x 5 mm²), doublet and/or triplet samples with the same laser conditions will be generated in order to allow all the planned characterizations.

Conclusions

In this deliverable, we have presented a detailed characterization of the as-grown SiGe layers that were available at the beginning of the project (cf. “first batch of samples”, deliverable D3.2, section 2, Fig. 1).

First, the results obtained from the undoped layers clearly indicated that the SiGe layers fabricated at CEA-Leti exhibited very good thickness and Ge concentration uniformities over the very vast majority of the wafer surface (300 mm wafers). It was also confirmed that the grown layers were perfectly strained (compressive) with no evidence of defects at the Si/SiGe interface or inside the epilayer. The perfect correspondence between the nominal and the effective wafer characteristics was also confirmed for all other undoped SiGe wafers from the same batch of samples.

In the second section, we proved the reliability of the process used to deposit compressively strained boron-doped SiGe layers on top of bulk Si by CVD with boron concentrations of: 7.0x10^{19} cm^{-3}, 1.3x10^{20} cm^{-3} and 2.3x10^{20} cm^{-3}. By characterizing these layers, we showed their good uniformity in thickness, Ge concentration and strain over 300 mm wafers. In addition, by combining Hall-effect measurements and SIMS chemical profiles, we evaluated activation rates to be close to 100 %, 80 % and 60 %, respectively. However, even in the presence of high fractions of electrically inactive boron, the carrier transport properties were not deteriorated compared to that in a fully activated doped layer.

These results demonstrated the need for improved activation processes when using really large amounts of boron in *in-situ* doped SiGe layers. In order to improve such fabrication process, while gaining a deeper insight in the dopant activation mechanism, a new Design-of Experiment was discussed and agreed within the consortium, the aim being to increase the activation rate of as-grown layers by performing different sets of post-epitaxy anneals. Details of the planned experiments were given in the third and last section of this report.

References

[1] J.M. Hartmann, L Clavelier, C Jahan, P Holliger, G Rolland, T Billon, C Defranoux, *Selective epitaxial growth of boron- and phosphorus-doped Si and SiGe for raised sources and drains*, Journal of Crystal Growth, Vol. 264, Issues 1–3, pp 36-47, 2004 (DOI:10.1016/j.jcrysgro.2003.12.055).

[2] M. Py, *Study of interfaces and nanometric structures by ToF-SIMS: upon a spatially resolved quantitative analysis*, PhD thesis, p. 277.

[3] J. M. Hartmann, A. Abbadie and S. Favier, *Critical thickness for plastic relaxation of SiGe on Si(001) revisited*, Journal of Applied Physics, Vol. 110, 083529, 2011 (DOI:10.1063/1.3656989).

[4] B. M. M. MCGregor, R. J. P. Lander, P. J. Phillips, E. H. C. Parker, T. E. Whall, *Temperature-dependent Hall scattering factor and drift mobility in remotely doped Si:B/SiGe/Si heterostructures*, Applied Physics Letters, Vol. 74, No. 9, pp. 1245-1247, 1999 (DOI:10.1063/1.123513).

[5] R. J. P. Lander, Y. V. Ponomarev, J. G. M. van Berkum, W. B. de Boer, R. Loo, M. Caymax, Drift mobilities and Hall scattering factors of holes in ultrathin $Si_{1-x}Ge_x$ layers ($0.3<x<0.4$) grown on Si, Journal of Applied Physics, Vol. 88, No. 4, pp. 2016-2023, 2000 (DOI:10.1063/1.1305555).

[6] P. Kinsler, W. Th. Wenckebach, Hall effect and ionized impurity scattering in $Si_{1-x}Ge_x$, Journal of Applied Physics, Vol. 94, No. 11, pp. 7159-7162, 2003 (DOI:10.1063/1.1622994).

[7] L. Romana, E. Napolitani, V. Privitera, S. Scalese, A. Terrasi, S. Mirabella, M. G. Grimaldi, *Carrier concentration and mobility in B doped* $Si_{1-x}Ge_x$, Materials Science and Engineering B, Vol. 102, Issues 1-3, pp. 49-52, 2003 (DOI:10.1016/S0921-5107(02)00621-9).

[8] F. Severac, *Jonctions ultra-minces p+/n pour MOS "ultimes": étude de l'impact des défauts cristallins sur la mobilité et l'activation du bore*, PhD thesis, pp. 82-88, 2009.

[9] R. Daubriac, *Characterization of alternative ion implantation techniques for the optimization of the source-drain module of FDSOI 28 nm technology*, PhD thesis, pp. 96-98, 2018.

[10] F. Severac *et al.*, J. Appl. Phys., 107 (2010) 123711 (DOI:10.1063/1.3446844).